IEEE Photonics Journal
An IEEE Photonics Society Publication

Open Access

Spin-Dependent Splitting Rotation of a Gaussian Beam Reflected From an Air–Glass Interface

Volume 11, Number 2, April 2019

Ting Wan
Shuoqing Liu
Zhaoming Luo
Li Min
Xiang Zhou
Yong Zhang

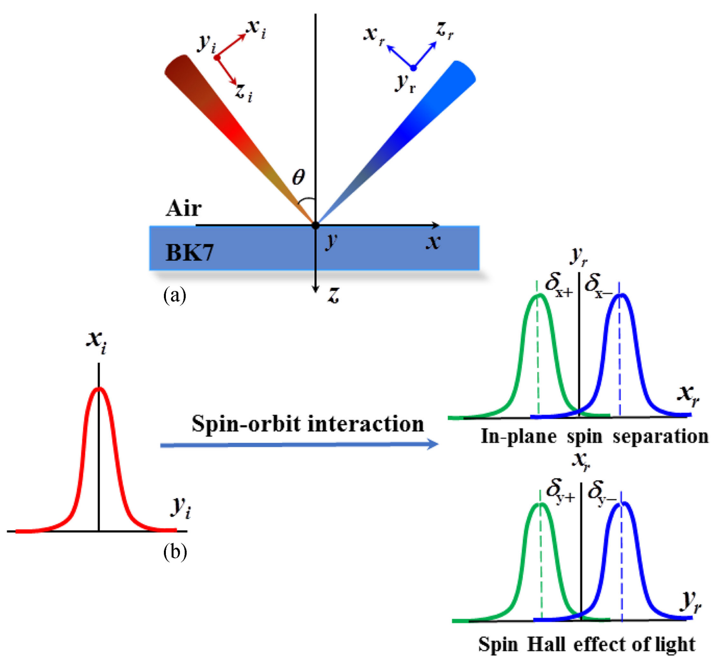

DOI: 10.1109/JPHOT.2019.2908963

Spin-Dependent Splitting Rotation of a Gaussian Beam Reflected From an Air–Glass Interface

Ting Wan, Shuoqing Liu, Zhaoming Luo, Li Min, Xiang Zhou, and Yong Zhang

College of Information and Communications Engineering, Hunan Institute of Science and Technology, Yueyang 414006, China

DOI:10.1109/JPHOT.2019.2908963

Manuscript received December 27, 2018; revised March 26, 2019; accepted March 29, 2019. Date of publication April 2, 2019; date of current version April 15, 2019. This work was supported in part by the Scientific Research Youth Project of Hunan Provincial Education Department under Grant 17B114, in part by the National Natural Science Foundation of China under Grant 61805078, in part by the Postgraduate Scientific Research Innovation Project of Hunan Province under Grant CX2018B775, and in part by the Science and Technology Program of Hunan Province, China, under Grant 2016TP1021.
(Ting Wan and Shuoqing Liu contributed equally to this work.) Corresponding author: Zhaoming Luo (e-mail: zhaomingluo@hnu.edu.cn).

Abstract: We investigate the spin-dependent splitting systematically by considering spin Hall effect of light and in-plane spin separation of light simultaneously, when a Gaussian beam is reflected from an air-glass interface. It is revealed that there exhibits a spin-dependent splitting rotation with the increase of the polarization angle, and the rotation direction and speed can be controlled by the incident angle. Remarkably, with the polarization angle increasing from 0° to 90°, the splitting rotates 180° clockwise in total when the incident angle is less than Brewster angle, whereas it rotates an angle under 90° counter-clockwise first and then clockwise return to the original position when the incident angle is larger than Brewster angle. Their initial rotation speeds of splitting to x_r direction both become larger as the incident angle approaches to Brewster angle, therefore when the incident angle is equal to Brewster angle, the splitting only forms a 90° clockwise rotation. These general laws of spin-dependent splitting rotation are demonstrated by instances, and the rotation behaviors are considered as a result of various proportions of transverse spin separation and in-plane spin separation. This research provides a feasible way to manipulate the photon spin in optical nanodevice.

Index Terms: Spin Hall effect of light, in-plane spin separation of light, splitting rotation.

1. Introduction

The spin Hall effect of light (SHEL) refers to that photons with opposite spin angular momenta will acquire transverse shifts and diverge from each other in the direction perpendicular to the incident plane, when a Gaussian beam propagates through an inhomogeneous medium, leading to the spin-dependent splitting [1]–[4]. The SHEL is essentially a polarization-dependent effect, whose origin is attributed to the spin-orbital interaction, and can be explained by the angular momenta conservation [5]–[8]. In a sense, SHEL can be regarded as a well-known transverse Imbert-Fedorov (IF) shift [9]–[11]. A similar spin-dependent splitting phenomenon in the incident plane, called in-plane spin separation of light (IPSSL), has also been found, which can be viewed as a kind of Goos-Hänchen (GH) shift [12], [13]. Above-mentioned spin-dependent splitting phenomena have attracted much attention because of the high scientific value and tremendous potential in application. Researchers have explored SHEL and IPSSL in various physical systems, such as high-energy physics [14], [15], semiconductor physics [16]–[19], optical physics [20], [21], metamaterials [22], [23] and plasmon physics [24]–[28].

In addition to the study of SHEL in different physical systems, people also have investigated it at medium interfaces, of which the typical one is air-glass interface. In 2008, Hosten and Kwiat used quantum weak measurement technology to observe spin Hall effect (SHE) of light refracted from an air-glass interface [29]. Since then, a lot of investigations on SHEL have been carried out at air-glass interface [30]–[36]. IF spatial shift of Gaussian beam reflected from an air-prism interface at the Brewster angle was studied and discussed [37], and some new spin-dependent splitting phenomena, such as spin angular-splitting [38], scattering-related spin-splitting [39] and asymmetric spin-splitting [40], [41], were discovered. In recent years, some researchers have begun to study the transaction properties by considering the SHEL and IPSSL simultaneously. Aiello *et al.* derived analytic expressions for GH and IF shifts [42], [43]. Pichugin *et al.* investigated the GH and IF shifts of higher-order Laguerre-Gaussian beams reflected from a dielectric slab [44]. Qin *et al.* comparatively analyzed transverse and in-plane spin separations, and mentioned the possible spin-dependent splitting rotation [10]. However, to our best knowledge, the phenomena of spin-dependent splitting rotation and their causes have not been systematically studied so far, nor their general laws have been obtained.

In this paper, we systematically investigate the spin-dependent splitting rotation of a Gaussian beam reflected from an air-glass interface by considering SHEL and IPSSL simultaneously. Firstly, on the basis of the planar angular spectrum theory, we establish a spin-dependent splitting model for describing beam propagation by introducing Stocks parameter S_3, and derive the expression of transverse and in-plane spin separations induced by SHEL and IPSSL of reflected beam. Secondly, we analyze the influences of polarization angle and incident angle on the total spin-dependent splitting theoretically, and the general laws of splitting rotation are found. Finally, we adopt instances to further demonstrate and analyze the general laws at $\theta = \theta_B$, $\theta < \theta_B$ and $\theta > \theta_B$.

2. Theoretical Analysis

Figure 1 illustrates the beam-propagation model of a Gaussian beam reflected from an air-glass interface. The z axis of laboratory Cartesian frame (x, y, z) is normal to the interface at $z = 0$, and coordinate frame (x_i, y_i, z_i) and (x_r, y_r, z_r) correspond to the incident and reflected electric fields. Here, the light beam is incident on the interface along z_i direction at incident angle θ and reflected along z_r direction. Remarkably, explicit spin-dependent splitting of reflected beam occurs in both x_r direction (the direction of IPSSL) and y_r direction (the direction of SHEL) as a result of the spin-orbital angular momentum interaction. δ_{y+} and δ_{y-} denote the transverse spin separation of left- and right-handed circularly, δ_{x+} and δ_{x-} represent the in-plane spin separation of left- and right-handed circularly, respectively. We consider a monochromatic Gaussian beam reflected from the air-glass interface, whose angular spectrum can be written as [45]

$$\widetilde{E}_i = \frac{w_0}{\sqrt{2\pi}} \exp\left[-\frac{w_0^2\left(k_{ix}^2 + k_{iy}^2\right)}{4}\right], \tag{1}$$

where w_0 is the beam waist, k_{ix} and k_{iy} denote the component of the wave vector of the incident beam in the direction of x_i and y_i respectively. The complex amplitude expression of a Gaussian beam based on the arbitrary angular spectrum in the electric field can be obtained by the Fourier transform as

$$E_a\left(x_a, y_a, z_a\right) = \int\int \widetilde{E}_a\left(k_{ax}, k_{ay}\right) \exp\left[i\left(k_{ax}x_a + k_{ay}y_a + k_{az}z_a\right)\right] dk_{ax}dk_{ay}. \tag{2}$$

Here, $a = i, r$ represent the incident and reflected beam. k_{ax}, k_{ay}, k_{az} are the components of the wave-vector k_a of the incident and reflected beam in x_a, y_a, z_a direction, and their relation is

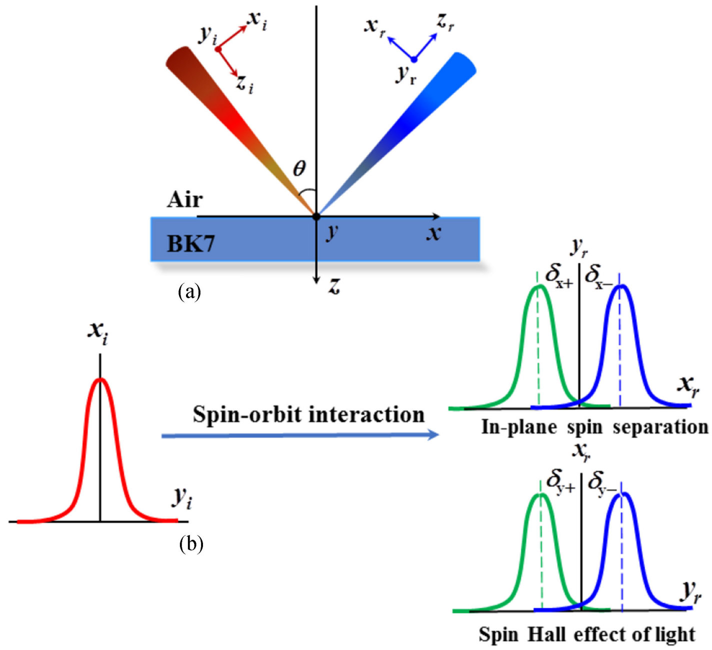

Fig. 1. (a) Schematic of a light beam reflected from the air-glass interface. Here θ is the incident angle. (b) Spin-dependent splitting induced by SHEL and IPSSL simultaneously. δ_{x+} and δ_{x-} denote the in-plane spin separations induced by the IPSSL for left- and right-handed circularly polarization, δ_{y+} and δ_{y-} represent the transverse spin separations induced by SHEL for left- and right-handed circularly polarization, respectively.

$k_{az} = \sqrt{k_a^2 - (k_{ax}^2 + k_{ay}^2)}$. $\widetilde{E}_r(k_{rx}, k_{ry})$ denotes the angular spectrum of reflected beam. To obtain the reflected filed, we can establish the relationship between incident and reflected angular spectrum by using the coordinate rotation. From the boundary condition, with the relationship between the incident and reflected wave-vector $k_{rx} = -k_{ix}$, $k_{ry} = -k_{iy}$, the reflected angular spectrum can be given by [40]

$$\begin{bmatrix} \widetilde{E}_r^H \\ \widetilde{E}_r^V \end{bmatrix} = \begin{bmatrix} r_p & \left(\frac{k_{ry}(r_p+r_s)\cot\theta}{k_0}\right) \\ -\left(\frac{k_{ry}(r_p+r_s)\cot\theta}{k_0}\right) & r_s \end{bmatrix} \begin{bmatrix} \widetilde{E}_i^H \\ \widetilde{E}_i^V \end{bmatrix}. \tag{3}$$

Here, $\widetilde{E}_r^H$, $\widetilde{E}_r^V$ and $\widetilde{E}_i^H$, $\widetilde{E}_i^V$ denote the angular spectrum for the horizontal (H) and vertical (V) polarizations of reflected and incident beam, respectively. r_s and r_p refer to the Fresnel reflection coefficients for the H and V polarized beam, $k_0 = 2\pi/\lambda$ is wave number in free space, and λ represents the wavelength. In general, the arbitrary linearly polarized beam can be viewed as an overlap of left- and right-handed polarized beam. Therefore, H and V polarization states can be written as follows,

$$\widetilde{E}^H = \frac{(\widetilde{E}_+ + \widetilde{E}_-)}{\sqrt{2}}, \tag{4}$$

$$\widetilde{E}^V = i\frac{(\widetilde{E}_- - \widetilde{E}_+)}{\sqrt{2}}, \tag{5}$$

where $\widetilde{E}_+$ and $\widetilde{E}_-$ indicate the angular spectrum of left- and right-handed polarized components. According to Eqs. (3)–(5), the expressions of the reflected angular spectrum can be defined as

$$\widetilde{E}_r^H = \frac{r_p}{\sqrt{2}}\left(\exp\left(ik_{ry}\delta_r^H\right)\widetilde{E}_{r+} + \exp\left(-ik_{ry}\delta_r^H\right)\widetilde{E}_{r-}\right), \tag{6}$$

$$\widetilde{E}_r^V = \frac{ir_s}{\sqrt{2}}\left(-\exp\left(ik_{ry}\delta_r^V\right)\widetilde{E}_{r+} + \exp\left(-ik_{ry}\delta_r^V\right)\widetilde{E}_{r-}\right). \tag{7}$$

Here, $\delta_r^H = (1 + r_s/r_p)\cot\theta/k_0$, $\delta_r^V = (1 + r_p/r_s)\cot\theta/k_0$. Remarkably, in expression (6) and (7), the term $\exp(\pm ik_{ry}\delta_r^{H,V})$ corresponds to the root cause of SHEL, namely, the spin-orbital interaction. Assumed that the polarization state of incident is arbitrary, which can be expressed by Jones matrix as $(\cos\gamma, \exp(i\phi)\sin\gamma)^T$. Here, ϕ illustrates the phase difference between the x and y polarized components ($\phi = 0$ corresponds to the linear polarization state), γ describes the azimuth angle of the light wave oscillation direction with respect to x direction. Substituting (6) and (7) into (4) and (5), we can get the reflected field distributions as follows,

$$\begin{aligned}\widetilde{E}_r^H = {} & \frac{k_0\omega_0\exp(ik_rz_r)}{2\sqrt{\pi}(R+iz_r)^3}\{[r_p(R+iz_r)^2 - ix(R+iz_r)\partial_\theta r_p]\cos\gamma \\ & + ye^{i\phi}\left[(iR - z_r)(r_p + r_s) + x\partial_\theta r_p\right]\cot\theta\sin\gamma\}\exp\left[-\frac{k_0(x_r^2+y_r^2)}{2(R+iz_r)}\right],\end{aligned} \tag{8}$$

$$\begin{aligned}\widetilde{E}_r^V = {} & \frac{k_0\omega_0\exp(ik_rz_r)}{2\sqrt{\pi}(R+iz_r)^3}\{y\left[(r_p + r_s)(-iR + z_r) - x\partial_\theta r_p\right]\cot\theta\cos\gamma \\ & + e^{i\phi}r_s(R+iz_r)^2\sin\gamma\}\exp\left[-\frac{k_0(x_r^2+y_r^2)}{2(R+iz_r)}\right],\end{aligned} \tag{9}$$

where $R = k_0w_0^2/2$ is the Rayleigh distance. It is well known that Stocks parameters S_3 can be used to indicate the circular polarization of light. $S_3 > 0$ and $S_3 < 0$ imply left- and right-handed elliptically polarized beam, $S_3 = +1$ and $S_3 = -1$ represent the left- and right-handed circularly polarized beam, respectively. Therefore the spin-dependent splitting can be intuitively represented by S_3 whose expression can be written as follow,

$$S_3 = 2|E_r^H||E_r^V|\sin\left[arg\left(E_r^V\right) - arg\left(E_r^H\right)\right]. \tag{10}$$

Here, $arg\left(E_r^H\right)$ and $arg\left(E_r^V\right)$ are the phases of reflected field for the H and V polarized beam. At discretionarily given transmission distance z_r, the centroid displacement expressions can be defined as follows,

$$\delta_{x\pm} = \frac{\int\int x_r I(x_r, y_r, z_r)dx_r dy_r}{\int\int I(x_r, y_r, z_r)dx_r dy_r}, \tag{11}$$

$$\delta_{y\pm} = \frac{\int\int y_r I(x_r, y_r, z_r)dx_r dy_r}{\int\int I(x_r, y_r, z_r)dx_r dy_r}, \tag{12}$$

where $I(x_r, y_r, z_r) \propto S_r \cdot e_{rz}$, namely, the electric field intensity distribution is proportional to the Poynting vector, and Poynting vector $S_r \propto Re[E_r^* \times H_r]$, magnetic field strength $H_r = -ik_r\nabla \times E_r$. Here, E_r represents electric field strength, E^* denotes the complex conjugate of the reflected field.

3. Results and Discussion

In this section, we will adopt the spin-dependent splitting model at an air-glass interface, as shown in Fig. 1, to study the optical transmission properties by considering the SHEL and IPSSL simultaneously in the case of linearly polarized incidence. We mainly focus on the influences of different polarization angles and incident angles on spin-dependent splitting. It is well known that there exists an amazing reflection behavior of the beam at Brewster angle θ_B, and different transmission properties are exhibited when incident angle θ is larger or less than θ_B [10], [46]. In the following

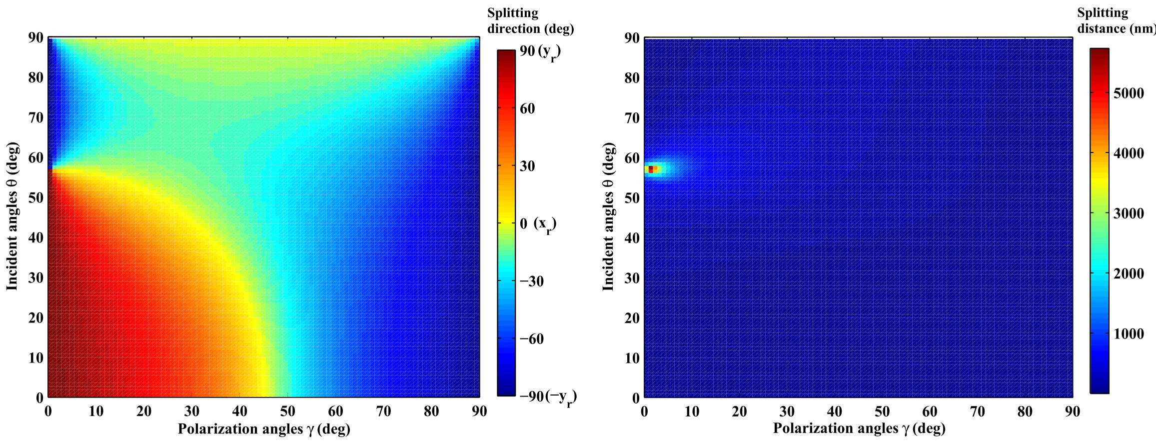

Fig. 2. Pseudo-color image of the (a) splitting direction angle and (b) splitting distance with different polarization angles γ and incident angles θ. The splitting direction can be described by the angle between the separation direction of right-handed circularly polarized component and x_r direction, and the splitting direction angles of 0°, 90° and -90° correspond to x_r, y_r and $-y_r$ directions, respectively.

simulations, we assume the refractive index of the glass to be 1.515, so that the Brewster angle in the interface is $\theta_B = 56.57^\circ$.

Firstly, we study the general laws on the spin-dependent splitting, the pseudo-color images of direction and distance of spin-dependent splitting with different polarization angles and incident angles are shown in Fig. 2. The splitting direction can be described by the angle between the separation direction of right-handed circularly polarized component and x_r direction, and the angle can be expressed as $180\,\arctan\left(\delta_y/\delta_x\right)/\pi$. On the basis of this expression, we can infer that the splitting direction angles of 0°, 90° and -90° correspond to x_r, y_r and $-y_r$ directions, respectively. From Fig. 2, we can verify that there exists an amazing reflection behavior of the beam and the direction and distance of spin-dependent splitting are supernormal near $\theta = \theta_B = 56.57^\circ$. Specifically, at $\theta < \theta_B$, the splitting direction forms a 180° clockwise rotation from y_r to x_r and then to $-y_r$ directions, and the more θ close to θ_B, the faster the splitting initially rotates to x_r direction. At $\theta > \theta_B$, the splitting rotates $\sim 180^\circ$ totally from $-y_r$ to x_r and then to $-y_r$ direction, and the initial rotation from $-y_r$ to x_r direction speeds up when θ close to θ_B or 90°. By the way, we mainly focus on studying the spin-dependent splitting near θ_B, so we do not discuss the phenomena at $\theta = 90^\circ$ in next works. Their initial rotational speeds of splitting to x_r direction both become larger as the θ approaches to θ_B, thus at $\theta = \theta_B$, the spin-dependent splitting forms a 90° clockwise rotation from x_r to $-y_r$ direction. In the following simulation, an attempt to further demonstrate these general laws and analyze their causes is done by instances at $\theta = \theta_B$, $\theta < \theta_B$ and $\theta > \theta_B$.

Secondly, we take instances to demonstrate the transmission laws of spin-dependent splitting at $\theta = \theta_B$. Figure 3 shows the intensity distributions of Stocks parameter S_3 at polarization angles $\gamma = 0^\circ$, 15°, 30°, 45°, 60° and 90°. It is revealed that there exists a spin-dependent splitting rotation clockwise from x_r to $-y_r$ direction with the increase of γ, which is consistent with the general laws obtained in Fig. 2(a). To explain the mechanism of this phenomenon, we also plot the dependence of spin-dependent displacements $\delta_{x,y\pm}$ induced by the SHEL and IPSSL on γ as shown in Fig. 4. We can find that with the increase of γ, for not only in-plane spin separation $\delta_{x\pm}$ but also transverse spin separation $\delta_{y\pm}$, the left- and right-handed circularly polarized components are equal in splitting magnitude while opposite in splitting direction. Thus we only need to consider the variation of the right-handed circularly polarized component in the following discussions. Combined with Fig. 3, we can conclude that the rotation is the result of the various proportions between in-plane spin separation and transverse spin separation. Specifically, at $\gamma = 0^\circ$, there appears a remarkable δ_{x+} but a tiny δ_{y+}, so that the IPSSL plays a dominant role comparing with SHEL, causing the spin-dependent splitting in x_r direction [see Fig. 3(a)]. With the increase of γ, δ_{x+} shows a significant

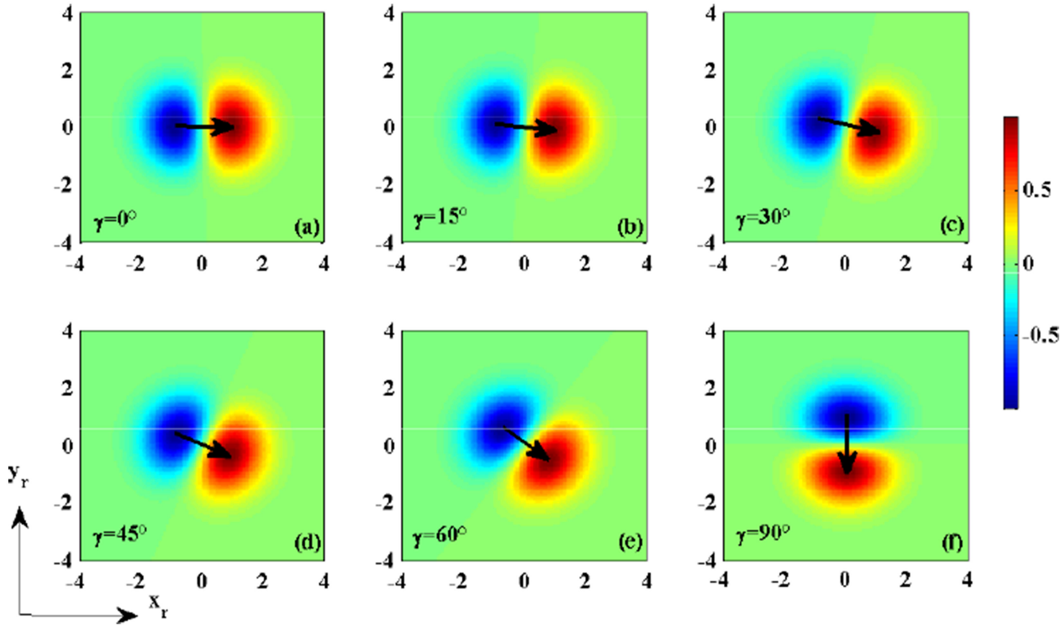

Fig. 3. Intensity distributions of Stocks parameter S_3 for incident angle $\theta = 56.67^\circ$ at different polarization angles: (a) $\gamma = 0^\circ$, (b) $\gamma = 15^\circ$, (c) $\gamma = 30^\circ$, (d) $\gamma = 45^\circ$, (e) $\gamma = 60^\circ$, (f) $\gamma = 90^\circ$, respectively. The arrows indicate the directions of spin-dependent splitting.

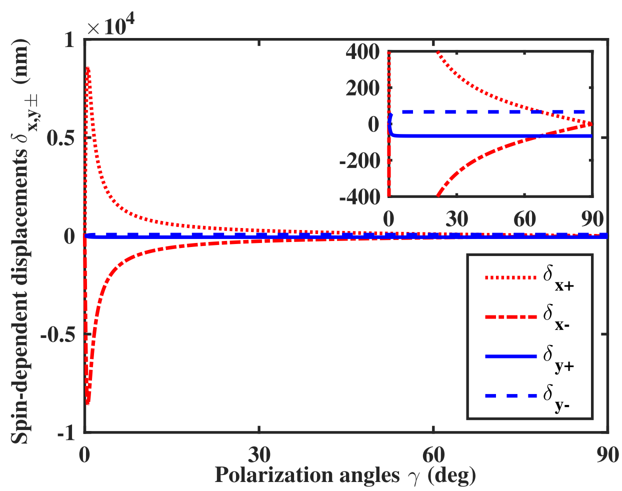

Fig. 4. Dependence of spin-dependent displacements $\delta_{x,y\pm}$ induced by the SHEL and IPSSL on the polarization angle γ for incident angle $\theta = 56.57^\circ$. The red dotted and dash-dotted lines denote in-plane spin separations of δ_{x+} and δ_{x-} induced by the IPSSL, and blue solid and dashed lines denote transverse spin separations of δ_{y+} and δ_{y-} induced by the SHEL, respectively.

exponential decrease but δ_{y+} remains stable, thus the proportion of the SHEL gradually grows, leading to the splitting rotates constantly [see Fig. 3(b)–(e)]. When γ increases to 90°, δ_{x+} keeps decreasing to 0, hence the SHEL replays a dominant role in the spin-dependent splitting and the splitting is in $-y_r$ direction [see Fig. 3(f)].

Thirdly, we demonstrate the transmission laws of spin-dependent splitting at $\theta < \theta_B$. Figure 4 describes the intensity distributions of Stocks parameter S_3 at $\gamma = 0^\circ$, 15°, 30°, 45°, 60° and 90° in the cases of $\theta = 30^\circ$ and 45°. It is found that there exists a 180° spin-dependent splitting rotation clockwise from y_r to x_r and then to $-y_r$ direction with the increase of γ, which is in good agreement

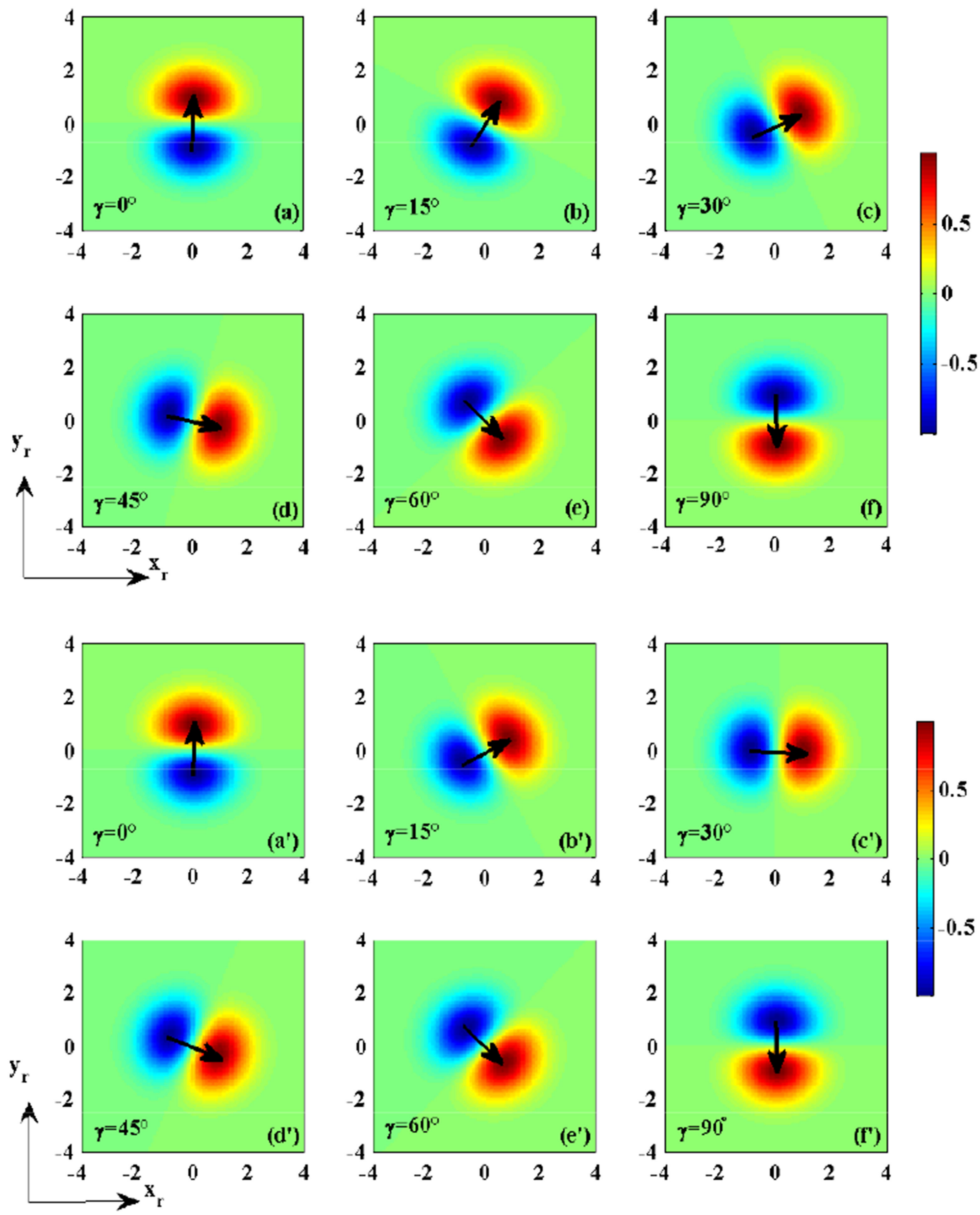

Fig. 5. Intensity distributions of Stocks parameter S_3 for incident angle $\theta = 30^\circ$ at different polarization angles: (a) $\gamma = 0^\circ$, (b) $\gamma = 15^\circ$, (c) $\gamma = 30^\circ$, (d) $\gamma = 45^\circ$, (e) $\gamma = 60^\circ$, (f) $\gamma = 90^\circ$, respectively. (a')–(f') the corresponding intensity distributions of Stocks parameter S_3 for incident angle $\theta = 45^\circ$.

with the general laws observed in Fig. 2(a). Comparing Fig. 5(a)–(f) with Fig. 5(a')–(f') we can find that the initial rotation from y_r to x_r direction speeds up as θ approaches to θ_B, thus for $\theta = \theta_B$ the initial rotation disappears, and the direction of splitting varies from y_r to x_r direction at $\gamma = 0^\circ$ [see Fig. 3(a)]. To analyze the cause of these interesting phenomena, we plot the dependence of the spin-dependent displacements δ_{x,y_+} induced by SHEL and IPSSL on polarization angle γ as shown in Fig. 6. We can find from Fig. 6 that the SHEL plays a dominant role at $\gamma = 0^\circ$ owing that the value of δ_{y+} is much larger than δ_{x+}, thus there emerges a splitting in y_r direction [see Fig. 5(a)]. When γ increases from 0° to about 29° (or 39°) for $\theta = 30^\circ$ (or 45°), δ_{y+} decreases to 0 and the proportion of the SHEL decreases constantly, so that the splitting rotates to x_r direction.

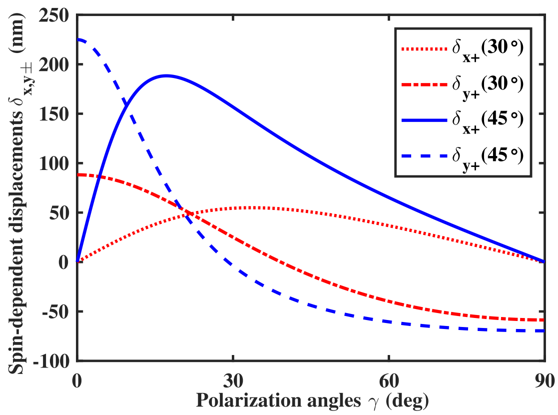

Fig. 6. Dependence of the spin-dependent displacements δ_{x,y_+} induced by SHEL and IPSSL for right-handed circularly polarized component on the polarization angle γ. The red dotted and dash-dotted lines denote δ_{x_+} and δ_{y_+} for the incident angle $\theta = 30^\circ$, and blue solid and dashed lines denote δ_{x_+} and δ_{y_+} for $\theta = 45^\circ$, respectively.

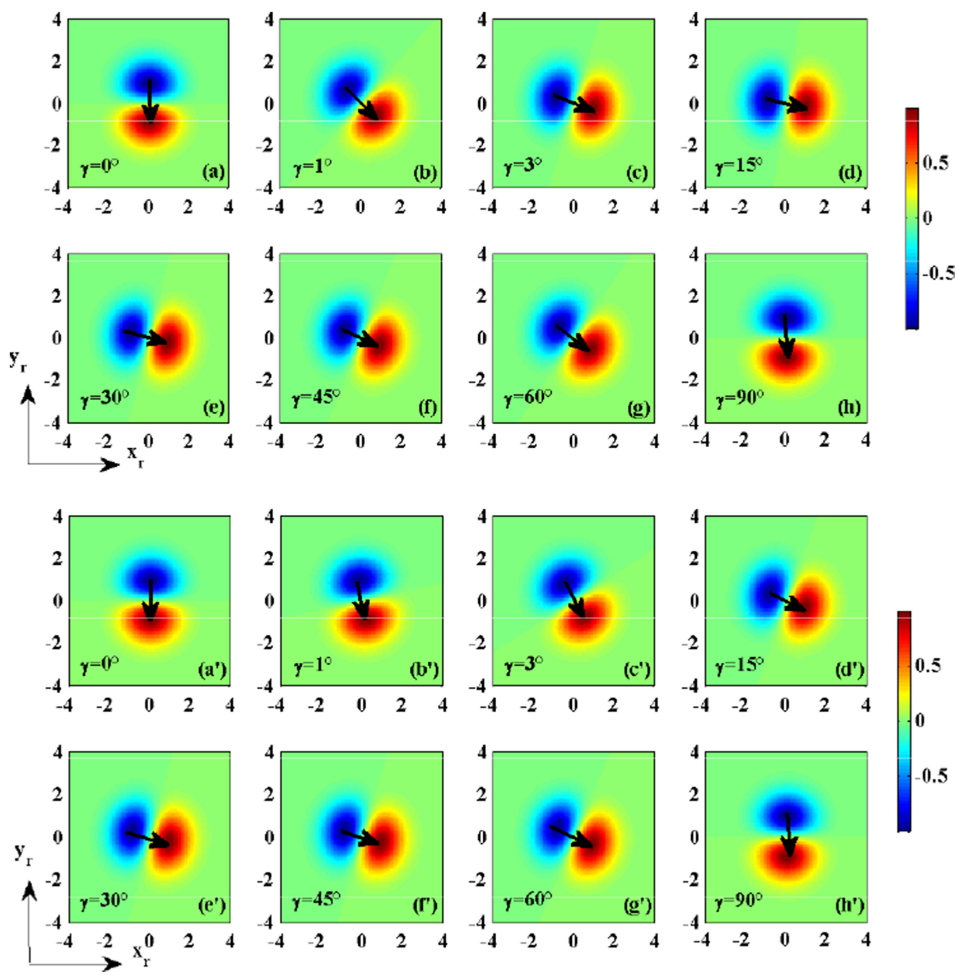

Fig. 7. Intensity distributions of Stocks parameter S_3 for incident angle $\theta = 58^\circ$ at different polarization angles: (a) $\gamma = 0^\circ$, (b) $\gamma = 1^\circ$, (c) $\gamma = 3^\circ$, (d) $\gamma = 15^\circ$, (e) $\gamma = 30^\circ$, (f) $\gamma = 45^\circ$, (g) $\gamma = 60^\circ$, (h) $\gamma = 90^\circ$, respectively. (a')–(h') the corresponding intensity distributions of Stocks parameter S_3 for incident angle $\theta = 70^\circ$.

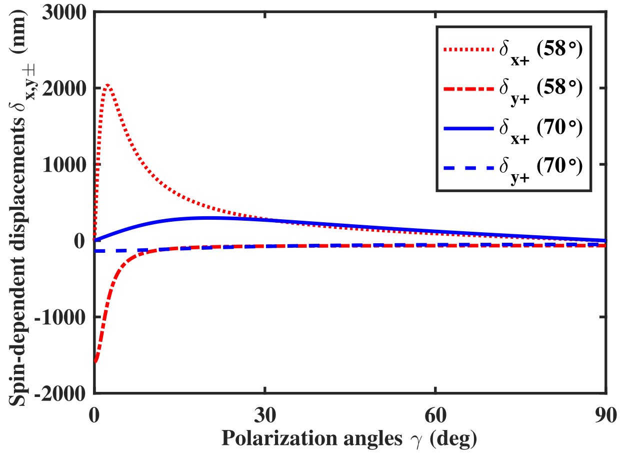

Fig. 8. Dependence of the spin-dependent displacements $\delta_{x,y+}$ induced by SHEL and IPSSL for right-handed circularly polarized component on the polarization angle γ. The red dotted and dash-dotted lines denote δ_{x+} and δ_{y+} for the incident angle $\theta = 58^\circ$, and blue solid and dashed lines denote δ_{x+} and δ_{y+} for $\theta = 70^\circ$, respectively.

As γ continually increases to 90°, there exists a spin accumulation reversal of the transverse spin separation induced by SHEL, which makes δ_{y+} grow oppositely, thus the splitting rotates clockwise from x_r to $-y_r$ direction. According to the above analyses, we can further prove that the spin-dependent splitting rotation is the result of the various proportions of δ_{x+} and δ_{y+} in the spin-dependent splitting with the increase of γ.

Finally, we demonstrate the transmission laws of spin-dependent splitting at $\theta > \theta_B$. Figure 7 displays the intensity distribution of Stocks parameter S_3 at different polarization angle $\gamma =$ 0°, 1°, 3°, 15°, 30°, 45°, 60° and 90° in the cases of $\theta = 58^\circ$ and 70°. It is found that the spin-dependent splitting rotates in a maximum angle counterclockwise from $-y_r$ to x_r direction and then returns to $-y_r$ direction with the increase of γ, which is in accordance with the general laws observed in Fig. 2(a). Comparing Fig. 7(a)–(h) with Fig. 7(a')–(h'), we can easily find that the spin-dependent splitting has a rapid initial rotation from $-y_r$ to x_r direction when θ is near to θ_B, thus for $\theta = \theta_B$ the initial rotation disappears, and the direction of splitting varies from $-y_r$ to x_r direction at $\gamma = 0^\circ$, which is consist with the circumstance in Fig. 3(a). To clarify the causes of these phenomena, we also plot the spin-dependent displacements $\delta_{x,y+}$ with the change of γ, as shown in Fig. 8. We can obtain that at θ of 58° (70°), δ_{x+} increases first and then decreases but δ_{y+} keeps decreasing, and spin accumulation reversal does not occur here, so that the splitting only conducts a rotation within 90°. Specifically, the SHEL plays a dominant role at $\gamma = 0^\circ$ due to δ_{x+} approximating to zero and δ_{y+} being a large negative value, hence the splitting concentrate at $-y_r$ direction [see Fig. 7(a) and (a')]. Similarly, with γ increases from 0° to 90°, δ_x shows a maximum value, leading to the splitting rotates counterclockwise in a maximum angle to x_r direction gradually. When γ increases to 90°, the SHEL regains its dominant role, therefore the splitting rotates clockwise and returns to $-y_r$ direction [see Fig. 7(h) and (h')]. Based on the above analysis, these phenomena can also be considered as the result of different proportions between in-plane spin separation and transverse spin separation.

4. Conclusion

In summary, we have established the spin-dependent splitting model of the linearly polarized beam reflected from an air-glass interface, and systematically investigated the influence laws of polarization angle and incident angle on spin-dependent splitting by considering the SHEL and IPSSL simultaneously. With the increase of polarization angle γ from 0° to 90°, the spin-dependent splitting occurs explicit rotation, and both the direction and speed of which can also be controlled by incident angle θ. Specifically, the splitting shows a 180° clockwise rotation from y_r to x_r and then to $-y_r$ direction at $\theta < \theta_B$. While at $\theta > \theta_B$, the final splitting shows a $\sim 180^\circ$ rotation in total, which rotates counterclockwise from $-y_r$ to x_r direction in a maximum angle less than 90° and returns clockwise to $-y_r$ direction. Their initial rotation speeds of spin-dependent splitting to x_r direction become larger as the incident angle θ approaches to Brewster angle θ_B, thus at $\theta = \theta_B$ the splitting only forms a 90° clockwise rotation from x_r to $-y_r$ direction. After getting these general laws, we then have adopted several instances to demonstrate the rotation behaviors of the spin-dependent splitting, and found these behaviors are the result of the various proportions between the transverse spin separation induced by the SHEL and in-plane spin separations induced by the IPSSL. These findings may provide a potential way to manipulate the spin of photons in optical nanodevices and even perform precision measurement of the polarization states.

References

[1] M. Onoda, S. Murakami, and N. Nagaosa, "Hall effect of light," *Phys. Rev. Lett.*, vol. 93, no. 8, Aug. 2004, Art. no. 083901.
[2] K. Y. Bliokh and Y. P. Bliokh, "Conservation of angular momentum, transverse shift, and spin Hall effect in reflection and refraction of an electromagnetic wave packet," *Phys. Rev. Lett.*, vol. 96, no. 7, Feb. 2006, Art. no. 073903.
[3] N. Hermosa, A. M. Nugrowati, A. Aiello, and J. P. Woerdman, "Spin Hall effect of light in metallic reflection," *Opt. Lett.*, vol. 36, no. 16, Aug. 2011, Art. no. 003200.
[4] L. Sheng *et al.*, "Sensitivity enhanced refractive index sensor by reducing the influence of in-plane wavevector in photonic spin hall effect," *IEEE Photon. J.*, vol. 10, no. 5, Sep. 2018, Art. no. 6501209.
[5] K. Y. Bliokh, F. J. Rodríguez-Fortuño, F. Nori, and A. V. Zayats, "Spin-orbit interactions of light," *Nature Photon.*, vol. 9, no. 12, pp. 796–808, Dec. 2015.
[6] H. Luo, S. Wen, W. Shu, and D. Fan, "Spin-to-orbital angular momentum conversion in spin Hall effect of light," *Opt. Commun.*, vol. 285, no. 6, pp. 864–871, Oct. 2011.
[7] T. Namba *et al.*, "Spin-orbit interaction in Pt or Bi2Te3 nanoparticle-decorated graphene realized by a nanoneedle method," *Appl. Phys.*, vol. 113, no. 5, Aug. 2018, Art. no. 053106.
[8] Z. Zhen *et al.*, "Measurement of giant spin splitting of reflected Gaussian beams," *IEEE Photon. J.*, vol. 10, no. 2, Dec. 2018, Art. no. 4500307.
[9] C. Imbert, "Calculation and experimental proof of the transverse shift induced by total internal reflection of a circularly polarized light beam," *Phys. Rev.*, vol. 5, no. 4, pp. 787–796, Feb. 1972.
[10] Y. Qin *et al.*, "Observation of the in-plane spin separation of light," *Opt. Exp.*, vol. 19, no. 10, pp. 9636–9645, May 2011.
[11] X. Ling *et al.*, "Recent advances in the spin Hall effect of light," *Rep. Prog. Phys.*, vol. 80, no. 6, Mar. 2017, Art. no. 066401.
[12] M. Gao, Z. Luo, H. Zhou, M. Chen, and J. Wu, "Precise control of Goos-Hänchen shift based on dielectric and graphene coating," *Chin. J. Lasers*, vol. 44, no. 7, Jul. 2017, Art. no. 0703019.
[13] M. A. Berbel, A. Cunillera, and R. Martínez-Herrero, "Goos-Hänchen and Imbert-Fedorov shifts: Relation with the irradiance moments of a beam," *J. Opt. Soc. Amer. A*, vol. 35, no. 2, pp. 286–292, Jan. 2018.
[14] P. Gosselin, A. Bérard, and H. Mohrbach, "Spin Hall effect of photons in a static gravitational field," *Phys. Rev. D*, vol. 75, no. 8, Apr. 2007, Art. no. 084035.
[15] C. A. Dartora *et al.*, "Lagrangian-Hamiltonian formulation of paraxial optics and applications: Study of gauge symmetries and the optical spin Hall effect," *Phys. Rev. A*, vol. 83, no. 1, Jan. 2011, Art. no. 012110.
[16] J. M. Ménard, A. E. Mattacchione, H. M. van Driel, C. Hautmann, and M. Betz, "Ultrafast optical imaging of the spin Hall effect of light in semiconductors," *Phys. Rev. B*, vol. 82, no. 4, Jul. 2010, Art. no. 045303.
[17] H. Luo *et al.*, "Enhancing or suppressing the spin Hall effect of light in layered nanostructures," *Phys. Rev. A*, vol. 84, no. 3, Sep. 2011, Art. no. 033801.
[18] X. Zhou, X. Ling, H. Luo, and S. Wen, "Identifying graphene layers via spin Hall effect of light," *Appl. Phys. Lett.*, vol. 101, no. 25, Dec. 2012, Art. no. 251602.
[19] M. H. Alizade and B. M. Reinhard, "Energence of transverse spin in optical modes of semiconductor nanowires," *Opt. Exp.*, vol. 24, no. 8, Apr. 2016, Art. no. 008471.
[20] O. Lafont *et al.*, "Controlling the optical spin Hall effect with light," *Appl. Phys. Lett.*, vol. 110, no. 6, Feb. 2017, Art. no. 061108.
[21] M. Cheng *et al.*, "Tunable and enhanced spin Hall effect of light in layered nanostructures containing graphene," *J. Opt. Soc. Amer. B*, vol. 35, no. 8, Jul. 2018, Art. no. 328897.
[22] M. Neugebauer, S. Grosche, S. Rothau, G. Leuchs, and P. Banzer, "Lateral spin transport in paraxial beams of light," *Opt. Lett.*, vol. 41, no. 15, pp. 3499, Jul. 2016.
[23] H. Zheng, C. Gao, M. Gao, and B. Guo, "Tunability of spin Hall effect of light with semiconductor metamaterial based on magneto-optical effects," *Opt. Quantum Electron.*, vol. 50, no. 7, Jun. 2018, Art. no. 073013.
[24] Y. Gorodetski *et al.*, "Weak measurements of light chirality with a plasmonic slit," *Phys. Rev. Lett.*, vol. 109, no. 7, Jul. 2012, Art. no. 013901.
[25] L. Salasnich, "Enhancement of four reflection shifts by a three-layer surface-plasmon resonance," *Phys. Rev. A*, vol. 86, no. 5, Nov. 2012, Art. no. 055801.
[26] X. Zhou and X. Ling, "Enhanced photonic spin Hall due to surface plasmon resonance," *IEEE Photon. J.*, vol. 8, no. 1, Feb. 2016, Art. no. 4801108.
[27] W. Zhu *et al.*, "The upper limit of the in-plane spin splitting of Gaussian beam reflected from a glass-air interface," *Sci. Rep.*, vol. 7, no. 1, Apr. 2017, Art. no. 1150.

[28] Q. Wang, X. Jiang, X. Wang, X. Dai, and Y. Xiang, “Enhancing photonic spin Hall effect in the surface planmon resonance structure covered by the graphene-MoS2 heterostructure,” *IEEE Photon. J.*, vol. 9, no. 6, Dec. 2017, Art. no. 6102610.

[29] O. Hosten and P. Kwiat, “Observation of the spin Hall effect of light via weak measurements,” *Science*, vol. 319, no. 5864, pp. 787–790, Feb. 2008.

[30] Y. Qin, Y. Li, H. He, and Q. Gong, “Measurement of spin Hall effect of reflected light,” *Opt. Lett.*, vol. 34, no. 17, pp. 2551–2253, Aug. 2009.

[31] H. Luo, X. Zhou, W. Shu, S. Wen, and D. Fan, “Enhanced and switchable spin Hall effect of light near the Brewster angle on reflection,” *Phys. Rev. A*, vol. 84, no. 4, Oct. 2011, Art. no. 043806.

[32] L. Kong *et al.*, “Spin Hall effect of reflected light from an air-glass interface around the Brewsters angle,” *Appl. Phys. Lett.*, vol. 100, no. 7, Feb. 2012, Art. no. 071109.

[33] J. Ren, B. Wang, Y. Xiao, Q. Gong, and Y. Li, “Direct observation of a resolvable spin separation in the spin Hall effect of light at an air-glass interface,” *Appl. Phys. Lett.*, vol. 107, no. 11, Sep. 2015, Art. no. 111105.

[34] C. Gao and B. Guo, “Tunable the spin Hall effect of light with graphene metamaterial,” *Optik*, vol 158, pp. 850–854, Apr. 2018.

[35] X. Qiu *et al.*, “Incident-polarization-sensitive and large in-plane-photonic-spin-splitting at the Brewster angle,” *Opt. Lett.*, vol. 40, no. 6, pp. 1018–1021, Mar. 2015.

[36] O. Takayama and G. Puentes, “Enhanced spin Hall effect of light by transmission in a polymer,” *Opt. Lett.*, vol. 43, no. 6, Mar. 2018, Art. no. 321342.

[37] L. Xie *et al.*, “Unveiling the spin Hall effect of light in Imbert-Fedorov shift at the Brewster angle with weak measurements,” *Opt. Exp.*, vol. 26, no. 18, pp. 22934–22943, Sep. 2018.

[38] X. Zhou, H. Luo, and S. Wen, “Weak measurements of a large spin angular splitting of light beam on reflection at the Brewster angle,” *Opt. Exp.*, vol. 20, no. 14, pp. 16003–16009, Jun. 2012.

[39] X. Qiu *et al.*, “Diffraction-dependent spin splitting in spin Hall effect of light on reflection,” *Opt. Exp.*, vol. 23, no. 15, pp. 18823–18831, Jul. 2015.

[40] X. Zhou and X. Ling, “Unveiling the photonic spin Hall effect with asymmetric spin-dependent splitting,” *Opt. Exp.*, vol. 24, no. 3, pp. 3025–3036, Feb. 2016.

[41] J. Zhang, Z. Luo, and H. Luo, “Steering asymmetric spin splitting in photonic spin Hall effect by orbital angular momentum,” *Acta. Opt. Sinica*, vol. 33, no. 11, Feb. 2016, Art. no. 1126002.

[42] A. Aiello and J. P. Woerdman, “Role of beam propagation in Goos-Hänchen and Imbert-Fedorov shifts,” *Opt. Lett.*, vol. 33, no. 13, pp. 1437–1439, Jun. 2008.

[43] K. Y. Bliokh and A. Aiello, “Goos-Hänchen and Imbert-Fedorov beam shifts: An overview,” *J. Opt.*, vol. 15, no. 1, Jan. 2013, Art. no. 014001.

[44] K. N. Pichugin, D. N. Maksimov, and A. F. Sadreev, “Goos-Hänchen and Imbert-Fedorov shifts of higher-order Laguerre-Gaussian beams reflected from a dielectric slab,” *J. Opt. Soc. Amer. A*, vol. 35, no. 8, pp. 1324–1329, Jul. 2018.

[45] T. Tang, Y. Zhang, J. Li, and L. Luo, “Spin hall effect enhancement of transmitted light through an anisotropic metamaterial slab,” *IEEE Photon. J.*, vol. 9, no. 4, Aug. 2017, Art. no. 4600910.

[46] M. Pan *et al.*, “Impact of in-plane spread of wave vectors on spin Hall effect of light around Brewsters angle,” *Appl. Phys. Lett.*, vol. 103, no. 7, Aug. 2013, Art. no. 071106.